Solution-Cast Monolayers of Cobalt Crown Ether Phthalocyanine on Highly Ordered Pyrolytic Graphite

Hao Lu,[†,‡] Iljo Kwak,[†,§,#] Jun Hong Park,[§,#] Katie O'Neill,[‡] Taniyuki Furuyama,[∥] Nagao Kobayashi,[∥] Alan Seabaugh,[‡] Andrew Kummel,[§] and Susan K. Fullerton-Shirey*[,‡,⊥]

[‡]Department of Electrical Engineering, University of Notre Dame, Notre Dame, Indiana 46556, United States
[§]Department of Chemistry and Biochemistry, [#]Materials Science & Engineering Program, University of California, San Diego, La Jolla, California 92093, United States
[∥]Department of Chemistry, Tohoku University, Sendai, Japan

🅢 *Supporting Information*

ABSTRACT: 15-Crown-5-ether-substituted cobalt(II) phthalocyanine (CoCrPc) is an atomically thin and flat-laying, electrically insulating molecule that can solvate ions; these properties are desirable for nanoelectronic devices. A simple, solution-phase deposition method is demonstrated to produce a monolayer of CoCrPc on highly ordered pyrolytic graphite (HOPG). A uniform and continuous CoCrPc layer is obtained on freshly cleaved HOPG by solution drop casting, followed by thermal annealing under ambient pressure in Ar in the temperature range of 150−210 °C. While the quality of the monolayer is independent of annealing time, the composition of the annealing atmosphere is critical; exposure to ambient air degrades the quality of the monolayer over the time scale of minutes. Using ultrahigh vacuum scanning tunneling microscopy, a highly ordered and flat CoCrPc layer with hexagonal symmetry and average spacing of 4.09 ± 0.2 nm is observed. The band gap of the CoCrPc, measured by scanning tunneling spectroscopy, is 1.34 ± 0.07 eV. The ability to prepare uniform, ordered, and conformal monolayers of CoCrPc molecules on HOPG represents the first step toward using these materials to seed dielectric growth on 2D crystals and provide a 2D electrolyte for the electrostatic gating of semiconductors at the ultimate limit of scaling.
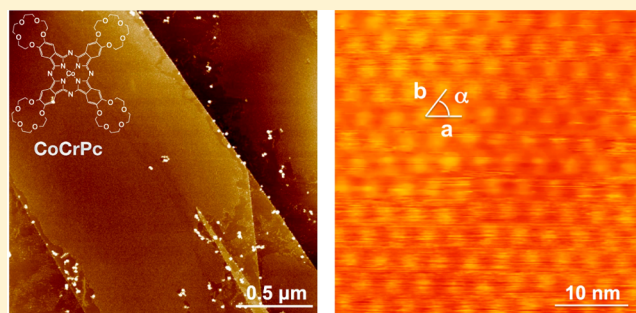
1. INTRODUCTION

Two-dimensional (2D) crystals, such as graphene, hexagonal boron nitride (h-BN), and transition metal dichalcogenides (TMDs), such as $MoTe_2$ and MoS_2, are potential candidates for future electronic devices, including TMD-based field-effect transistors (FETs) and tunnel FETs (TFETs).[1−4] High performance transistors based on 2D crystals require thin and defect-free gate dielectrics. However, due to the absence of dangling bonds, 2D semiconductors are generally unreactive, thereby making the deposition of dielectrics on the surface of these materials challenging. One approach to address this problem is the deposition of a seed layer onto which a gate dielectric is deposited.[5−12]

In addition to gate dielectrics, electronic devices based on 2D crystals also require doping methods. There are three common approaches to doping: substitutional, charge transfer, and electrostatic doping using either a metal gate or ions. Substitutional doping changes the optical band gap and can introduce defects that degrade electrical performance.[13] Charge transfer dopants, which rely on molecular physisorption, including NO_x,[14] SiN_x,[15] K,[16] and benzyl viologen,[17] are currently being explored. Similar to metal gates, ionic liquids and solid polymer electrolytes do not involve charge transfer,

but instead rely on electrostatics to induce image charge in the semiconductor. Electrolytes such as DEME-TFSI (N,N-diethyl-2-methoxy-N-methylethanaminium), EMIM-TFSI (1-ethyl-3-methylimidazolium bis(trifluoromethylsulfonyl)imide), and poly(ethylene oxide) with $LiClO_4$ or $CsClO_4$ have been used extensively for reconfigurable doping of graphene[18−20] and TMDs.[21−31] For basic research and development purposes, ionic liquids and polymer electrolytes are easy to use and enable higher capacitance density than a conventional oxide gate dielectric. However, due to their poor scalability to nanometer thicknesses and incompatibility with conventional photolithography, liquid and polymer electrolytes are unsuitable for 2D devices at the limit of scaling. Therefore, a solid electrolyte that is both 2D and can be deposited layer-by-layer is highly desirable.

To address the needs for dielectric deposition and electrolyte doping of 2D crystals, a flat-lying and insulating molecule is needed that can be deposited conformally with monolayer precision and can solvate alkali cations, such as Li^+. One such

class of molecules is crown-ether-substituted phthalocyanine (Pc). Among the various crown ether metal Pc (MPc) molecules that can be obtained via peripheral substitution, 15-crown-5-ether-substituted cobalt(II) phthalocyanine (CoCrPc), as shown in Figure 1, can solvate cations smaller
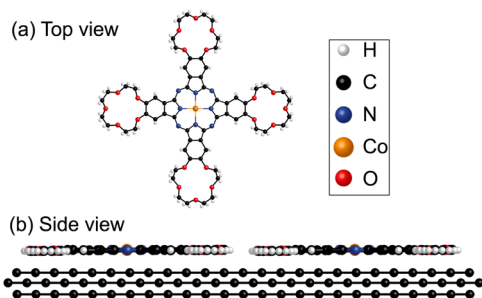
Figure 1. (a) Schematic diagram of the chemical structure of 15-crown-5-ether-substituted cobalt(II) phthalocyanine (CoCrPc) and (b) schematic side view of CoCrPc on HOPG.

than the cavity size of the crown ethers and can lay flat on the substrate.[32,33] The metal atom of the MPc interacts strongly with the substrate,[32,33] enabling the use of MPcs to seed atomic layer deposition (ALD) growth of high-κ dielectrics.[34,35] When the MPc molecule is functionalized with crown ethers, such as CoCrPc, the molecule can solvate various alkali cations,[33,36] providing a potential doping strategy for 2D crystals.

MPcs and their derivatives can be deposited in an ultrahigh vacuum (UHV) by molecular beam epitaxy (MBE) onto Au(111),[37] graphene,[38−40] and TMDs[34] to form perfectly ordered monolayers. Because of their excellent film growth and electronic properties,[41] an MPc monolayer can be used to nucleate ALD of wide band gap oxides, such as Al_2O_3.[34,35] Although MBE deposition of MPcs allows for precise control of layer thickness for use as a crystalline multilayer, a monolayer of MPcs also can be prepared by simple solution phase deposition, which is more practical for commercial application compared to MBE, because solution deposition can be done at atmospheric pressure. For example, Kong et al. prepared a monolayer of TiOPc by drop casting from solution (1 μM TiOPc in toluene) onto freshly cleaved, highly ordered pyrolytic graphite (HOPG) and Au(111) under ambient conditions and performed scanning tunneling microscopy (STM) measurements.[42] Their STM observations revealed that TiOPc molecules form a hexagonally packed monolayer on both substrates.

Previously, Yoshimoto and co-workers prepared a CoCrPc monolayer on both Au(100) and (111) and characterized the surfaces with STM.[32,33] The CoCrPc monolayer was formed by immersing the Au substrate for 5 min in a benzene−ethanol (9:1 v/v) solution saturated with CoCrPc, followed by an ultrapure water rinse. STM measurements of the CoCrPc, made in 0.05 M $HClO_4$, confirmed that the molecules form an ordered, flat-lying array parallel to the Au surface and the CoCrPc layer had 4-fold symmetry, with spacing of 2.5 nm.[32,33] They also showed that the crown ether moieties of CoCrPc can trap Ca^{2+} by making molecule−ion pairs. The imaging was performed in solution, where solvent−CoCrPc interactions may help stabilize the CoCrPc and facilitate the formation of a monolayer. In addition, strong interactions between the Au substrate and the phthalocyanine molecules may help to promote monolayer formation more than phthalocyanine deposited on a graphene substrate.[39]

In this report, the solution phase deposition of a CoCrPc monolayer on HOPG is presented. The monolayer was prepared by solution drop casting, followed by annealing in Ar at ambient pressure. Because both HOPG and graphene share the same surface chemistry, originating from sp³ hybridization, it is reasonable to regard HOPG and graphene as equivalent for the purposes of this study. The solution deposition and annealing conditions were optimized by characterizing the surfaces with atomic force microscopy (AFM). Using UHV-STM, the surface morphology and the packing structure of the monolayer were observed at the molecular level, and scanning tunneling spectroscopy (STS) was used to directly probe the band gap of the monolayer.[43]

2. EXPERIMENTAL DETAILS

CoCrPc was synthesized following a previously published procedure.[33] Because the crown ether ligands make the molecule hygroscopic,[44] monolayer deposition and AFM characterization were performed inside an Ar-filled glovebox (O_2 and water < 0.1 ppm) and anhydrous solvents were used. A total of 1.3 mg CoCrPc was dissolved in a 100 mL mixture of anhydrous benzene−ethanol (9:1 v/v, Sigma-Aldrich: 99.8% anhydrous benzene, 99.5% anhydrous ethanol). To improve CoCrPc dispersion in the solvent, the solution was enclosed in a glass vial with a screw-top lid, removed from the glovebox, and sonicated for 60 min at 40 kHz (Branson Sonicator 2510). The solution was returned to the glovebox for sample preparation.

CoCrPc monolayers were deposited onto HOPG by drop casting from solution followed by thermal annealing in an Ar-filled glovebox. The CoCrPc solution was deposited onto 1.2 × 1.2 cm pieces of HOPG (2 mm thick, ZYB grade, Bruker) using a micropipettor with a drop volume of 25 μL. Scotch tape (3M) was used to cleave the HOPG. Subsequent drops were applied after the previous drop evaporated and the sample surface appeared dry. After drop casting, the sample was transferred onto a hot plate and annealed in the temperature range of 120−500 °C in an Ar ambient. After 30 min of annealing, the samples were transferred through an airlock into the second bay of the glovebox for atomic force microscopy (AFM) measurements without air exposure.

To determine how the quality of the CoCrPc monolayer depends on air exposure, the solution was drop cast onto a freshly cleaved HOPG surface, dried in the glovebox, and then brought into air for annealing. The same sample was annealed on the hot plate at 150 °C for 5, 10, 15, and 35 min, and after each annealing period, the sample was returned to the glovebox for AFM measurements.

The topography of CoCrPc monolayer was characterized using AFM (Dimension Icon Scanning Probe Microscope, Bruker) in ScanAsyst/PeakForce Tapping mode with silicon nitride ScanAsyst-air probes (Bruker). During the characterization, the box light and glovebox circulation were turned off to minimize noise. Line profiles were used to measure the thickness of a CoCrPc monolayer on a sample prepared with partial surface coverage.

Monolayer formation of CoCrPc was confirmed by STM. After drop casting 2 drops on freshly cleaved HOPG, the sample was annealed in a N_2-filled convection oven (Carbolite 301) for 20 min at 180 °C at ambient pressure. The sample was immediately loaded into an Omicron multichamber ultrahigh vacuum system with base pressure less than 1 × 10⁻¹⁰ Torr. The sample topography was observed with a VT-STM
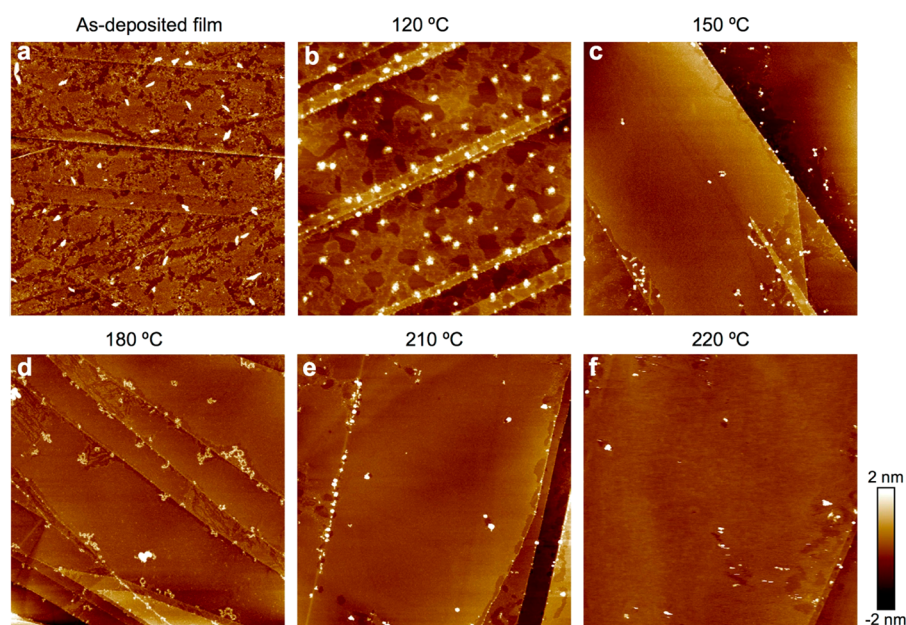
Figure 2. AFM images of a 15-crown-5-ether-substituted cobalt(II) phthalocyanine (CoCrPc) monolayer on HOPG prepared by drop casting 34 μL/cm^2 of 13 mg/L CoCrPc benzene−ethanol (9:1 v/v) solution: (a) As-deposited film, (b) annealed in Ar for 30 min at 120, (c) 150, (d) 180, (e) 210, and (f) 220 °C. All images are 2 × 2 μm^2. The white particles are likely CoCrPc aggregates. Line scans of (a)−(c) are shown in Figures S1−S3 in the Supporting Information.

(Omicron Nanotechnology) with tungsten tips made by electrochemically etching a tungsten wire. All STM images were acquired in constant current mode (I = 0.2 nA) with a sample bias of −1.8 V. STS was used to measure the band gap of monolayer CoCrPc using a variable z-mode with external lock-in amplifier in the sample bias range from −1.5 to 1.5 V. In addition, a bare HOPG surface was measured as a control.

3. RESULTS AND DISCUSSION

3.1. Surface Morphology of the CoCrPc Monolayer and Annealing Temperature Window. After drop casting and solvent evaporation, the annealing temperature was varied between 120 and 500 °C to determine the optimum temperature range for obtaining a CoCrPc monolayer. The annealing time was fixed at 30 min; however, the quality of the CoCrPc monolayer was insensitive to annealing time in the range of 5 to 60 min. A total of two 25 μL drops (34 μL/cm^2) provide full coverage on a 1.44 cm^2 HOPG surface. AFM images of the CoCrPc, as deposited on HOPG and after 30 min of annealing at five temperatures between 120−220 °C, are shown in Figure 2. Large particles line the step edges of the HOPG and are scattered randomly on the mesas. The lateral particle size and height vary between 10−100 nm and 1−10 nm, respectively. The particles are either impurities or undissolved CoCrPc aggregates; it is more likely that the particles are aggregates because their size and density decrease with annealing temperature.

The as-deposited film (Figure 2a) shows uneven coverage of CoCrPc. After annealing at 120 °C, full coverage is not achieved (Figure 2b); however, the CoCrPc thickness is at least one monolayer, as shown by line scans in Figure S2 with step heights of ~0.5 nm. Note that the shape of the large particles changes from irregular to spherical after annealing at 120 °C. Annealing in the temperature range of 150−210 °C (Figure 2c−e) yields nearly complete CoCrPc coverage on the mesas as the CoCrPc film becomes continuous and uniform. The

continuity of the CoCrPc film is broken along the mesa edges and near the particles. The dose of CoCrPc was optimized to provide the minimum amount of material required to cover the area of the HOPG substrate without observable CoCrPc vacancy islands (i.e., a single monolayer). When the dose of CoCrPc is insufficient to cover the entire area of the HOPG substrate, discontinuous islands are formed with veins joining them. Figure 3 represents an extreme case for which the dose is
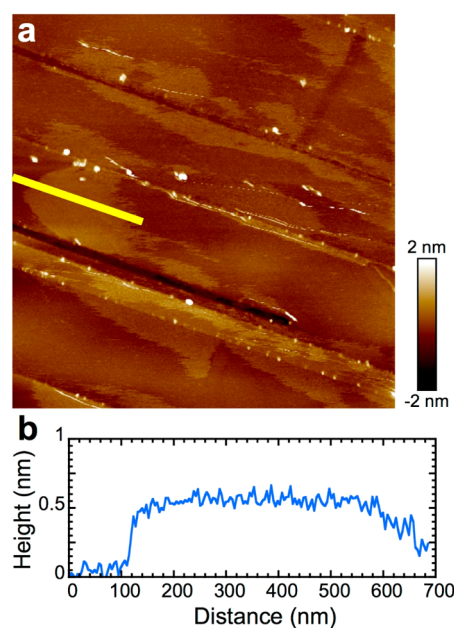
Figure 3. AFM of CoCrPc monolayer with partial coverage: (a) 2 × 2 μm^2 AFM image of CoCrPc monolayer with partial surface coverage by depositing 8 μL/cm^2 of 13 mg/L CoCrPc benzene−ethanol (9:1 v/v) solution and Ar annealing at 150 °C for 30 min and (b) line scan corresponding to the yellow line in part (a).
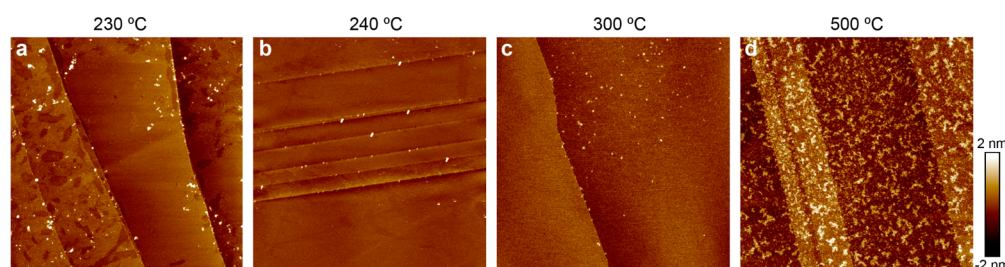
Figure 4. AFM images of degrading CoCrPc monolayer on HOPG. The CoCrPc monolayer was prepared by drop casting 34 μL/cm^2 of 13 mg/L CoCrPc benzene−ethanol (9:1 v/v) and (a) annealed in Ar for 30 min at 230, (b) 240, (c) 300, and (d) 500 °C. All images are 2 × 2 μm^2. A line scan of (d) is shown in Figure S3 in the Supporting Information.
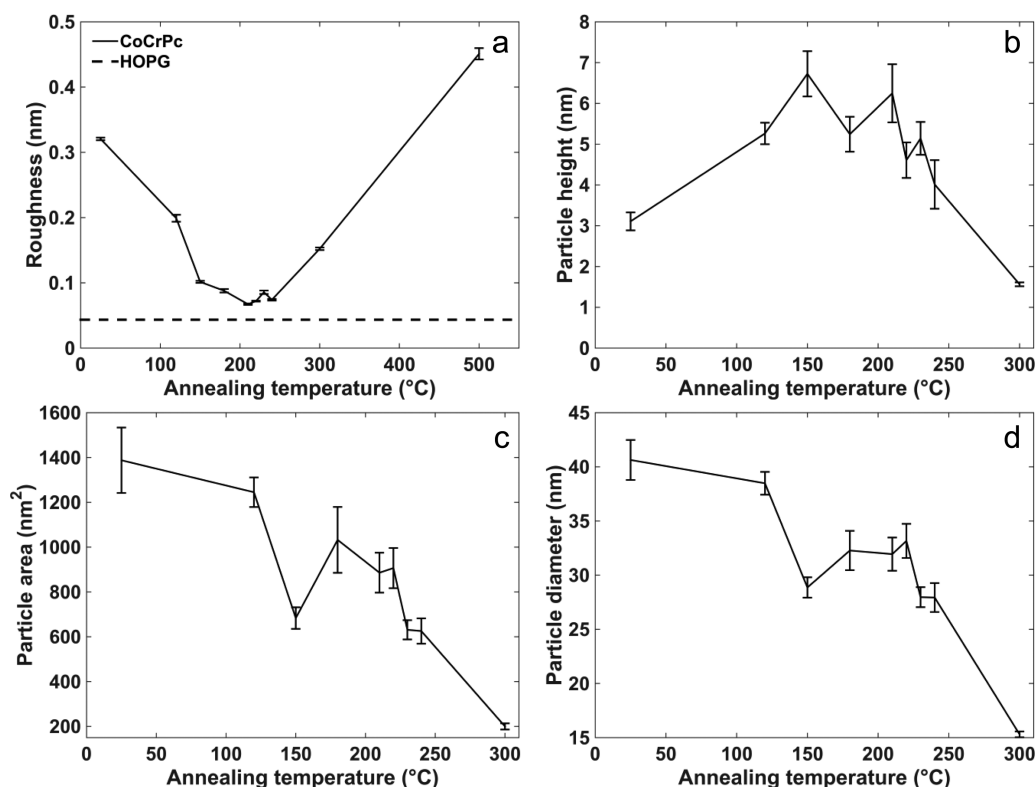
Figure 5. Statistical analysis of as-deposited and annealed CoCrPc from AFM scans in Figures 2 and 4. (a) Root mean squared roughness (R_q) of bare HOPG and as-deposited and annealed CoCrPc within the temperature range of 120−500 °C ($n = 5$). The roughness data is taken on the mesa where a continuous CoCrPc monolayer is formed. (b) Particle height, (c) area, and (d) diameter of CoCrPc annealed within the temperature range of 120−300 °C. All errors are standard errors.

so small that isolated CoCrPc patches are formed. When the dose of CoCrPc exceeds that needed for a single monolayer, a second layer of islands start to form, nucleating primarily at the step edges of the HOPG substrate. When the annealing temperature increases beyond 210 °C, the upper bound of the optimal annealing temperature window is reached, and the quality of the CoCrPc film starts to deteriorate (Figure 2f).

To measure the thickness of a single CoCrPc layer after 150 °C anneal, 12 μL of CoCrPc solution (8 μL/cm^2) was used to intentionally provide incomplete coverage (Figure 3a). The thickness of the layer, 0.46 ± 0.01, nm is quantified by averaging 10 line scan over a large CoCrPc island (Figure 3b). This agrees with the thickness of an individual CoCrPc molecule measured by STM (0.42 nm),[33] indicating that the CoCrPc molecules lie flat on the HOPG surface. The line scan also indicates that the CoCrPc forms a uniform monolayer over the distance of the line scan.

Within the annealing window of 150−210 °C, the quality of the coverage and the layer thickness are insensitive to temperature. However, as mentioned above, at an annealing temperature of 220 °C, the CoCrPc monolayer becomes inhomogeneous. The monolayer continues to degrade with increasing temperature, as shown by the AFM scans in Figure 4, where the annealing temperature is varied from 230 to 500 °C. Specifically, the presence of large, nonspherical aggregates is observed at $T > 300$ °C. It is expected that the ether bonds in the crowns of the CoCrPc decompose at $T > 300$ °C, further contributing to the significant change in the surface morphology at $T = 500$ °C.

The surface roughness is quantified as a function of temperature in Figure 5a by averaging over five area scans of size 0.3 × 0.3 μm^2. At temperatures below 210 °C, the surface roughness decreases with increasing annealing temperature by a factor of ∼4; however, at temperatures larger than 240 °C, surface roughness increases by a factor of ∼6 as the CoCrPc

21995
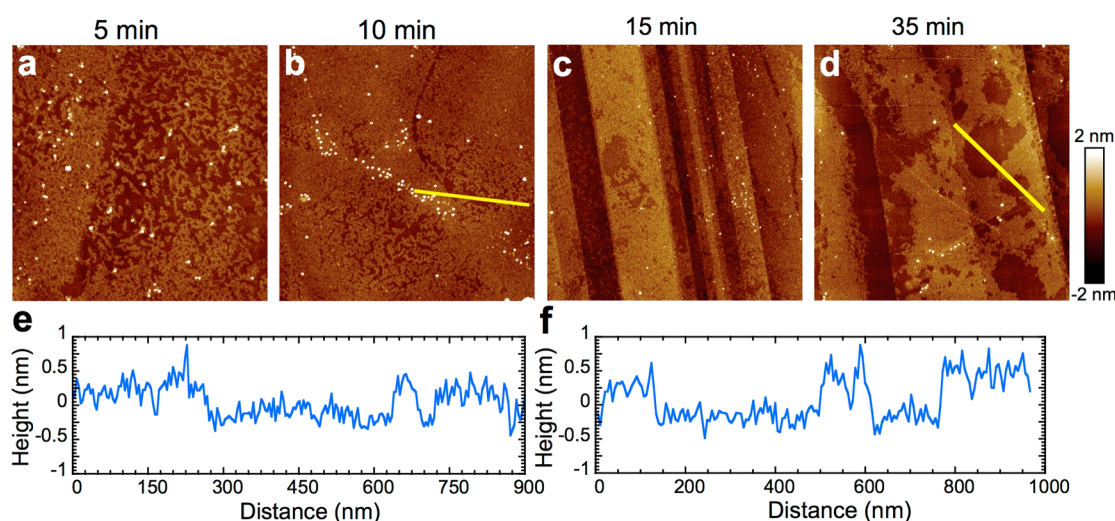
Figure 6. AFM images of a CoCrPc monolayer after air anneal. A thin CoCrPc film was prepared on HOPG by drop casting 34 μL/cm^2 of 13 mg/L CCP benzene–ethanol (9:1 v/v) solution and (a) annealed in air at 150 °C for 5 min, (b) an additional 5 min, (c) an additional 5 min, and (d) an additional 20 min. The total annealing time is 5, 10, 15, and 35 min. (e) Line scan following the yellow line in AFM image (b), and (f) line scan following the yellow line in image (d). All AFM images are 2 × 2 μm^2.
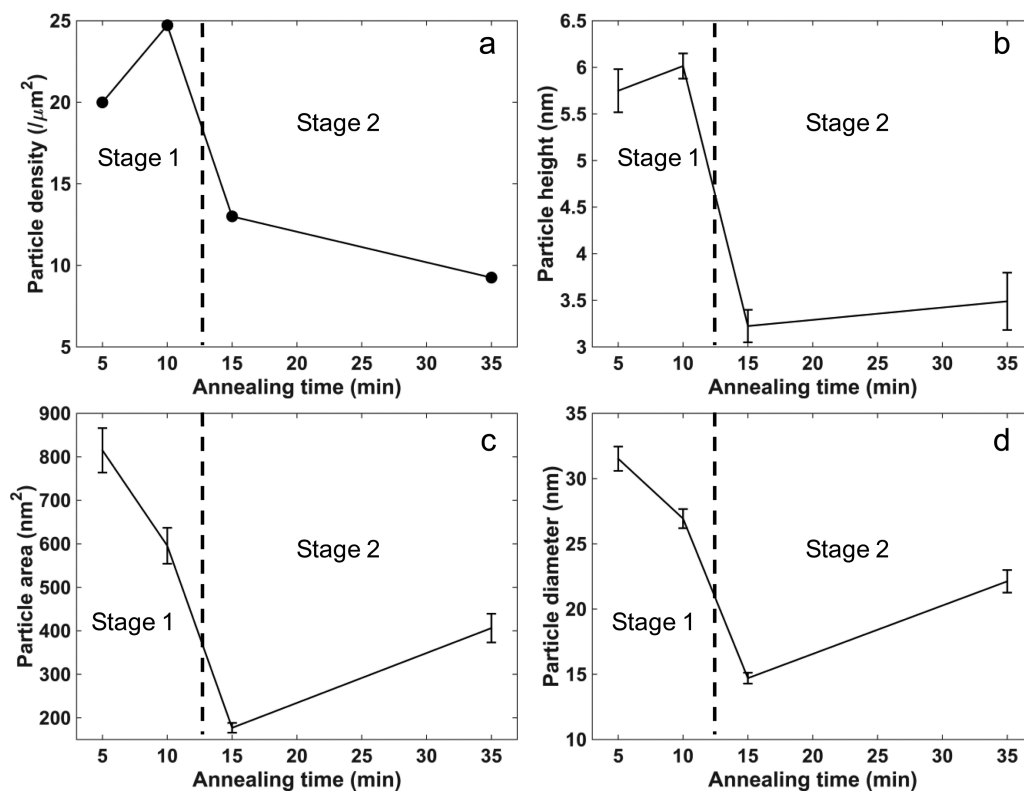
Figure 7. Statistical analysis of particle density and size observed in Figure 6 as a function of annealing time in air: (a) particle density, (b) height, (c) area, and (d) diameter of CoCrPc annealed in air at 150 °C. All errors are standard errors.

molecules rearrange and aggregate. It is possible that the CoCrPc molecules are partially desorbing from the surface at $T \geq 240$ °C, contributing to the increased surface roughness.

In addition to surface roughness, the height, area, and diameter of the spherical particles observed at $T \leq 300$ °C are quantified in Figure 5b–d by averaging over all particles in the AFM images in Figures 2 and 4a–c. Generally, the size of the spherical particles decreases with increasing temperature, suggesting that they are aggregates of CoCrPc. The scan at 500 °C is excluded from the analysis because, at high

temperature, the molecules acquire sufficient thermal energy that they aggregate into nonspherical clusters that are significantly larger than the size of the original aggregates observed at $T \leq 300$ °C.

3.2. Effect of Air Exposure. To characterize the stability of the CoCrPc films in air, samples were prepared in Ar by drop casting without annealing, then transferred from the glovebox and annealed in air at 150 °C for varying amounts of time. As shown in Figure 6, the quality of the CoCrPc monolayer degrades significantly compared to samples prepared under Ar
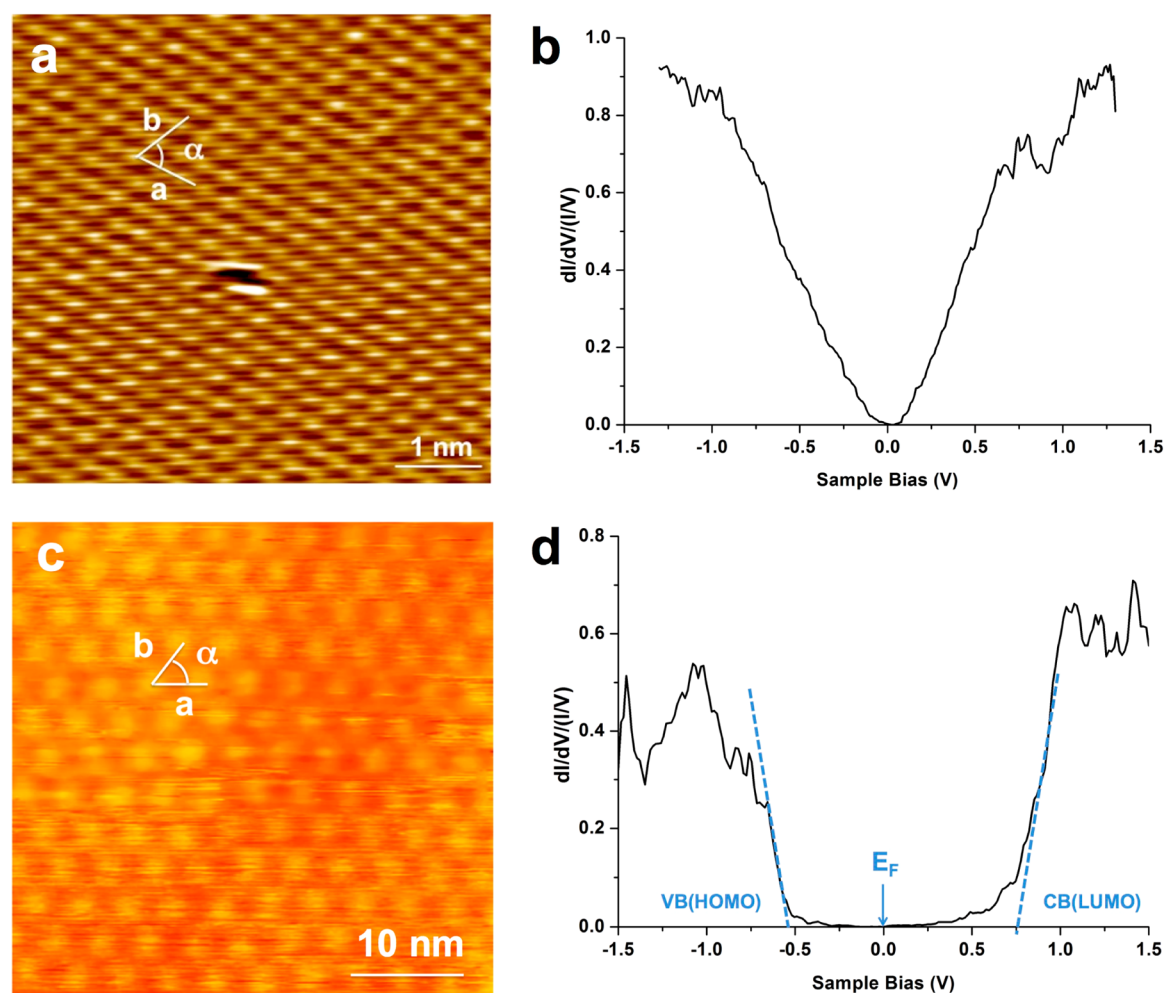
Figure 8. STM and STS of HOPG and drop cast and annealed CoCrPc on HOPG. (a) STM image of a bare HOPG surface with lattice parameters $a = 0.22 \pm 0.07$ nm, $b = 0.21 \pm 0.1$ nm, and $\alpha = 58 \pm 2°$. STM was measured with $V_{sample} = -1.8$ V and $I_t = 0.2$ nA at -180 °C. (b) STS $dI/dV/(I/V)$ spectra (average of 20 measurements) of a bare HOPG sample showing no apparent energy gap. (c) Filled-state STM image of a CoCrPc monolayer on HOPG with lattice parameters $a = b = 4.08 \pm 0.2$ nm, $\alpha = 59 \pm 1°$. A highly ordered and flat CoCrPc layer with hexagonal lattice structure is observed. (d) STS $dI/dV/(I/V)$ spectra of a CoCrPc layer on HOPG. STS curve shows that the CoCrPc layer has a 1.34 ± 0.07 eV band gap. E_F is the position of Fermi energy level, located at 0 V.

annealing. The morphology of the CoCrPc monolayer changes dramatically when the annealing time increases from 5−10 min to 15−35 min. Because of the morphological similarity of the images before 10 min and after, Figure 5a and b are denoted as annealing stage 1, and Figure 5c and d are denoted as annealing stage 2. In annealing stage 1, instead of forming a continuous monolayer, the CoCrPc molecules form clusters, some of which have small spacing, ∼10 nm, and some large spacing, ∼50−100 nm. In annealing stage 2, the CoCrPc clusters form a film that is more continuous, but rough. As a result, large areas (∼0.5 μm) with less CoCrPc coverage are created. As shown in the line scans in Figure 6e and f, the thickness of CoCrPc film is measured as 0.46 ± 0.03 nm (stage 1) and 0.46 ± 0.12 nm (stage 2) by averaging five line scans. The standard error of the measured thickness of CoCrPc film annealed in air is 3 to 12 times larger than those annealed in Ar, further indicating that the quality of the monolayer has degraded.

The size and density of the spherical particles also change significantly upon exposure to air while annealing. Based on the AFM scans in Figure 6, the particle density, height, area and diameter are quantified in Figure 7 by averaging over all particles in Figure 6a−d. The particle density decreases by a

factor of 2 between annealing stage 1 and stage 2. In addition, the particles in annealing stage 2 are smaller in height, area, and diameter than those in annealing stage 1. Even when a sample is deposited and annealed in the glovebox, postannealing air exposure at room temperature will degrade the quality of the CoCrPc monolayer (Figure S4 in Supporting Information), consistent with metal phthalocyanines ability of bond oxidizing molecules.[45]

3.3. STM and STS. UHV STM was employed to confirm that CoCrPc lies flat on HOPG. As mentioned above, a flat-lying CoCrPc molecule is required for both seeding ALD growth of high-κ gate dielectrics and electrostatic doping via ions located in the crowns. Using the same method as described in the above AFM studies, 2 drops of 10 mg/L CoCrPc in anhydrous benzene−ethanol (9:1 v/v) were drop cast onto freshly cleaved HOPG and annealed in 1 atm of N_2 at 180 °C for 20 min. Note that the samples were transferred in air to the STM and outgassed in UHV at 3×10^{-10} Torr for 10 min. In addition, a bare HOPG surface was measured as a control. Figure 8a shows a topographic STM image of bare HOPG, with lattice parameters $a = 0.22 \pm 0.07$ nm, $b = 0.21 \pm 0.1$ nm, and $\alpha = 58 \pm 2°$; the typical hexagonal symmetry of carbon atoms is

observed. Figure 8c is a STM image of a solution casted CoCrPc layer on HOPG, where a highly ordered and flat CoCrPc layer is observed with hexagonal symmetry. This packing arrangement is different from the quadratic packing geometry of CoCrPc deposited on Au(100) and (111),[32,33] consistent with the substrate controlling the packing geometry of MPc molecules. However, in contrast to CoCrPc, TiOPc packs hexagonally on both HOPG and Au(111), indicating that both the identity of the MPc and the substrate control packing geometry.[42] Kong et al. showed that unit cell parameters of TiOPc on HOPG and Au(111) substrates are similar: $a = b = 1.3 \pm 0.1$ nm, $\alpha = 60 \pm 1°$; and $a = b = 1.0 \pm 0.2$ nm, $\alpha = 60 \pm 2°$, respectively.[42] In the present study, the unit cell length of CoCrPc on HOPG is significantly larger, $a = b = 4.08 \pm 0.2$ nm, $\alpha = 59 \pm 1°$, than TiOPc on HOPG. This is due, in part, to the larger size of CoCrPc; however, the CoCrPc spacing is also larger than the previously reported spacing of CoCrPc on Au(111), 2.5 nm.[33] The lower packing density of CoCrPC on HOPG compared to Au(111) is attributed to weaker binding between CoCrPC and HOPG due to the lower electron density of HOPG compared to Au.[39] In contrast, the negligible spacing change for TiOPc on both HOPG and Au is likely the consequence of a much stronger molecule−substrate binding interaction due to the large dipole of TiOPc.[46]

Using STS, the normalized differential conductivity ($dI/dV/(I/V)$) of the bare HOPG and CoCrPc layer are measured as a function of scan voltage (V), as shown in Figures 8b and d. For the sample covered in CoCrPc, the STS data were measured on the center of the CoCrPc molecules. The scan bias was swept from −1.5 to 1.5 V. A total of 20 STS curves were obtained from different points and averaged to estimate the band gap. The $dI/dV/(I/V)$ curve obtained on the bare HOPG surface is shown in Figure 8b. The curve has a parabolic shape, indicating there is no apparent energy gap due to the high conductivity of the HOPG sample. In contrast, the energy band gap is clearly observed in the sample covered by CoCrPc (Figure 8d). The locations of the valence-band maximum (E_V) and conduction-band minimum (E_C) are determined by assuming linear onsets in the differential conductance in Figure 8d. Straight lines are drawn through the spectra on either side of an onset, and the band edge onset position is obtained by the intersection of the lines and horizontal axis. The data indicate a valence band edge (left) and conduction band edge (right) at −0.58 ± 0.04 and 0.76 ± 0.03 eV, respectively, giving a band gap of 1.34 ± 0.07 eV.

To our knowledge, this is the first reported measurement of the band gap of CoCrPc with STS. This small band gap is similar to previously reported values for other metal phthalocyanines on an HOPG substrate.[39,47,48] For example, Park et al. reported a band gap of 1.75 eV for single layer copper phthalocyanine (CuPc) on HOPG.[39] They also show that the band gap depends on the number of layers: multilayer CuPc film has a band gap of 2.3 eV. The fact that the STS measurements in Figure 8d are uniform across the entire scan area also supports the assertion that the CoCrPc coverage is a single monolayer.

4. CONCLUSION

A monolayer of CoCrPc was deposited on HOPG by simple drop casting from solution followed by thermal annealing in Ar under ambient pressure. The effects of annealing temperature and air exposure on the CoCrPc layer were characterized. A uniform and continuous film was obtained by Ar annealing in the temperature range of 150−210 °C, nearly independent of annealing time. However, the quality and coverage of the CoCrPc layer degraded over time by air annealing, and when the sample was exposed to air after argon annealing. Therefore, an inert environment is needed to maintain the quality of the monolayer on HOPG. STM shows that the CoCrPc monolayer lays flat on the HOPG surface with hexagonal symmetry, and for the first time, the band gap of the CoCrPc monolayer was measured by STS. This study lays the groundwork for using a monolayer of CoCrPc molecules in nanoelectronic devices as an ion conductor or as a seeding layer for ALD growth on 2D crystals. When complexed with alkali cations, the CoCrPc molecules could be used as a 2D electrolyte for electrostatic doping or memory in 2D crystals.

■ ASSOCIATED CONTENT

ⓢ Supporting Information

The Supporting Information is available free of charge on the ACS Publications website at DOI: 10.1021/acs.jpcc.5b05233.

> Line scans of as-deposited CoCrPc and annealed at 120 °C; line scans and roughness of bare HOPG, and CoCrPc annealed at 150 and 500 °C; AFM of Ar-annealed CoCrPc after 15 min and 48 h of air exposure (PDF)

■ AUTHOR INFORMATION

Corresponding Author
*Phone: +1 (412) 624-2079. E-mail: fullerton@pitt.edu.

Present Address
⊥Department of Chemical and Petroleum Engineering, University of Pittsburgh, Pittsburgh, PA, U.S.A. (S.K.F.-S.).

Author Contributions
†These authors contributed equally (H.L. and I.K.).

Notes
The authors declare no competing financial interest.

■ REFERENCES

(1) Das, S.; Prakash, A.; Salazar, R.; Appenzeller, J. Toward Low-Power Electronics: Tunneling Phenomena in Transition Metal Dichalcogenides. ACS Nano 2014, 8, 1681−1689.

(2) Fiori, G.; Bonaccorso, F.; Iannaccone, G.; Palacios, T.; Neumaier, D.; Seabaugh, A.; Banerjee, S. K.; Colombo, L. Electronics Based on Two-Dimensional Materials. Nat. Nanotechnol. 2014, 9, 768−779.

(3) Jena, D. Tunneling Transistors Based on Graphene and 2-D Crystals. Proc. IEEE 2013, 101, 1585−1602.

(4) Wang, Q. H.; Kalantar-Zadeh, K.; Kis, A.; Coleman, J. N.; Strano, M. S. Electronics and Optoelectronics of Two-Dimensional Transition Metal Dichalcogenides. Nat. Nanotechnol. 2012, 7, 699−712.

(5) Alaboson, J. M.; Wang, Q. H.; Emery, J. D.; Lipson, A. L.; Bedzyk, M. J.; Elam, J. W.; Pellin, M. J.; Hersam, M. C. Seeding Atomic Layer Deposition of High-κ Dielectrics on Epitaxial Graphene with Organic Self-Assembled Monolayers. ACS Nano 2011, 5, 5223−5232.

(6) Farmer, D. B.; Chiu, H. Y.; Lin, Y. M.; Jenkins, K. A.; Xia, F.; Avouris, P. Utilization of a Buffered Dielectric to Achieve High Field-Effect Carrier Mobility in Graphene Transistors. Nano Lett. 2009, 9, 4474−4478.

(7) Kim, S.; Nah, J.; Jo, I.; Shahrjerdi, D.; Colombo, L.; Yao, Z.; Tutuc, E.; Banerjee, S. K. Realization of a High Mobility Dual-Gated Graphene Field-Effect Transistor with Al_2O_3 Dielectric. *Appl. Phys. Lett.* **2009**, *94*, 062107.

(8) Lee, B.; Park, S.-Y.; Kim, H.-C.; Cho, K.; Vogel, E. M.; Kim, M. J.; Wallace, R. M.; Kim, J. Conformal Al_2O_3 Dielectric Layer Deposited by Atomic Layer Deposition for Graphene-Based Nanoelectronics. *Appl. Phys. Lett.* **2008**, *92*, 203102.

(9) McDonnell, S.; Brennan, B.; Azcatl, A.; Lu, N.; Dong, H.; Buie, C.; Kim, J.; Hinkle, C. L.; Kim, M. J.; Wallace, R. M. HfO_2 on MoS_2 by Atomic Layer Deposition: Adsorption Mechanisms and Thickness Scalability. *ACS Nano* **2013**, *7*, 10354−10361.

(10) Sangwan, V. K.; Jariwala, D.; Filippone, S. A.; Karmel, H. J.; Johns, J. E.; Alaboson, J. M.; Marks, T. J.; Lauhon, L. J.; Hersam, M. C. Quantitatively Enhanced Reliability and Uniformity of High-κ Dielectrics on Graphene Enabled by Self-Assembled Seeding Layers. *Nano Lett.* **2013**, *13*, 1162−1167.

(11) Shin, W. C.; Bong, J. H.; Choi, S. Y.; Cho, B. J. Functionalized Graphene as an Ultrathin Seed Layer for the Atomic Layer Deposition of Conformal High-K Dielectrics on Graphene. *ACS Appl. Mater. Interfaces* **2013**, *5*, 11515−11519.

(12) Wang, X.; Tabakman, S. M.; Dai, H. Atomic Layer Deposition of Metal Oxides on Pristine and Functionalized Graphene. *J. Am. Chem. Soc.* **2008**, *130*, 8152−8153.

(13) Gong, Y.; et al. Band Gap Engineering and Layer-by-Layer Mapping of Selenium-Doped Molybdenum Disulfide. *Nano Lett.* **2014**, *14*, 442−449.

(14) Zhao, P.; et al. Air Stable p-Doping of WSe_2 by Covalent Functionalization. *ACS Nano* **2014**, *8*, 10808−10814.

(15) Chen, K.; Kiriya, D.; Hettick, M.; Tosun, M.; Ha, T. J.; Madhvapathy, S. R.; Desai, S.; Sachid, A.; Javey, A. Air Stable n-Doping of WSe_2 by Silicon Nitride Thin Films with Tunable Fixed Charge Density. *APL Mater.* **2014**, *2*, 092504.

(16) Fang, H.; Tosun, M.; Seol, G.; Chang, T. C.; Takei, K.; Guo, J.; Javey, A. Degenerate n-Doping of Few-Layer Transition Metal Dichalcogenides by Potassium. *Nano Lett.* **2013**, *13*, 1991−1995.

(17) Kiriya, D.; Tosun, M.; Zhao, P.; Kang, J. S.; Javey, A. Air-Stable Surface Charge Transfer Doping of MoS_2 by Benzyl Viologen. *J. Am. Chem. Soc.* **2014**, *136*, 7853−7856.

(18) Das, A.; et al. Monitoring Dopants by Raman Scattering in an Electrochemically Top-Gated Graphene Transistor. *Nat. Nanotechnol.* **2008**, *3*, 210−215.

(19) Efetov, D. K.; Kim, P. Controlling Electron-Phonon Interactions in Graphene at Ultrahigh Carrier Densities. *Phys. Rev. Lett.* **2010**, *105*, 256805.

(20) Efetov, D. K.; Maher, P.; Glinskis, S.; Kim, P. Multiband Transport in Bilayer Graphene at High Carrier Densities. *Phys. Rev. B: Condens. Matter Mater. Phys.* **2011**, *84*, 161412.

(21) Lin, M.-W.; Liu, L.; Lan, Q.; Tan, X.; Dhindsa, K. S.; Zeng, P.; Naik, V. M.; Cheng, M. M.-C.; Zhou, Z. Mobility Enhancement and Highly Efficient Gating of Monolayer MoS_2 Transistors with Polymer Electrolyte. *J. Phys. D: Appl. Phys.* **2012**, *45*, 345102.

(22) Pu, J.; Yomogida, Y.; Liu, K. K.; Li, L. J.; Iwasa, Y.; Takenobu, T. Highly Flexible MoS_2 Thin-Film Transistors with Ion Gel Dielectrics. *Nano Lett.* **2012**, *12*, 4013−4017.

(23) Zhang, Y.; Ye, J.; Matsuhashi, Y.; Iwasa, Y. Ambipolar MoS_2 Thin Flake Transistors. *Nano Lett.* **2012**, *12*, 1136−1140.

(24) Perera, M. M.; Lin, M. W.; Chuang, H. J.; Chamlagain, B. P.; Wang, C.; Tan, X.; Cheng, M. M.; Tomanek, D.; Zhou, Z. Improved Carrier Mobility in Few-Layer MoS_2 Field-Effect Transistors with Ionic-Liquid Gating. *ACS Nano* **2013**, *7*, 4449−4458.

(25) Yuan, H. T.; et al. Zeeman-Type Spin Splitting Controlled by an Electric Field. *Nat. Phys.* **2013**, *9*, 563−569.

(26) Zhang, Y. J.; Ye, J. T.; Yomogida, Y.; Takenobu, T.; Iwasa, Y. Formation of a Stable *p-n* Junction in a Liquid-Gated MoS_2 Ambipolar Transistor. *Nano Lett.* **2013**, *13*, 3023−3028.

(27) Allain, A.; Kis, A. Electron and Hole Mobilities in Single-Layer WSe_2. *ACS Nano* **2014**, *8*, 7180−7185.

(28) Chuang, H. J.; Tan, X.; Ghimire, N. J.; Perera, M. M.; Chamlagain, B.; Cheng, M. M.; Yan, J.; Mandrus, D.; Tomanek, D.; Zhou, Z. High Mobility WSe_2 *p*- and *n*-Type Field-Effect Transistors Contacted by Highly Doped Graphene for Low-Resistance Contacts. *Nano Lett.* **2014**, *14*, 3594−3601.

(29) Lezama, I. G.; Ubaldini, A.; Longobardi, M.; Giannini, E.; Renner, C.; Kuzmenko, A. B.; Morpurgo, A. F. Surface Transport and Band Gap Structure of Exfoliated $2H-MoTe_2$ Crystals. *2D Mater.* **2014**, *1*, 021002.

(30) Zhang, Y. J.; Oka, T.; Suzuki, R.; Ye, J. T.; Iwasa, Y. Electrically Switchable Chiral Light-Emitting Transistor. *Science* **2014**, *344*, 725−728.

(31) Xu, H.; Fathipour, S.; Kinder, E. W.; Seabaugh, A. C.; Fullerton-Shirey, S. K. Reconfigurable Ion Gating of $2H-MoTe_2$ Field-Effect Transistors Using Poly(Ethylene Oxide)-$CsClo_4$ Solid Polymer Electrolyte. *ACS Nano* **2015**, *9*, 4900−4910.

(32) Yoshimoto, S.; Suto, K.; Itaya, K.; Kobayashi, N. Host-Guest Recognition of Calcium by Crown-Ether Substituted Phthalocyanine Array on Au(111): Relationship between Crown Moieties and Gold Lattice. *Chem. Commun.* **2003**, 2174−2175.

(33) Yoshimoto, S.; Suto, K.; Tada, A.; Kobayashi, N.; Itaya, K. Effect of Adlayer Structure on the Host−Guest Recognition between Calcium and Crown-Ether-Substituted Phthalocyanine Arrays on Au Single-Crystal Surfaces. *J. Am. Chem. Soc.* **2004**, *126*, 8020−8027.

(34) Park, J. H.; Kwak, I.; Sardashti, K.; Kaufman-Osborn, T.; Park, S. W.; Kummel, A. C. Ultrathin Titanyl Phthalocyanine Monolayers on Graphene for Dielectrics and Ordered ALD Nucleation. 2014 MRS Spring Meeting and Exhibit, San Francisco, CA, April 21−25, 2014, Materials Research Society: Warrendale, PA, 2014.

(35) Fathipour, S.; Park, J. H.; Kummel, A.; Seabaugh, A. Low-Leakage WSe_2 FET Gate-Stack Using Titanyl Phthalocyanine Seeding Layer for Atomic Layer Deposition of Al_2O_3. 2015 Dev. Res. Conf., Columbus, OH, June 21−24, 2015, Materials Research Society: Warrendale, PA, 2014.

(36) De, S.; Boda, A.; Ali, S. M. Preferential Interaction of Charged Alkali Metal Ions (Guest) within a Narrow Cavity of Cyclic Crown Ethers (Neutral Host): A Quantum Chemical Investigation. *J. Mol. Struct.: THEOCHEM* **2010**, *941*, 90−101.

(37) Cheng, Z. H.; Gao, L.; Deng, Z. T.; Liu, Q.; Jiang, N.; Lin, X.; He, X. B.; Du, S. X.; Gao, H. J. Epitaxial Growth of Iron Phthalocyanine at the Initial Stage on Au(111) Surface. *J. Phys. Chem. C* **2007**, *111*, 2656−2660.

(38) Wang, S. D.; Dong, X.; Lee, C. S.; Lee, S. T. Orderly Growth of Copper Phthalocyanine on Highly Oriented Pyrolytic Graphite (HOPG) at High Substrate Temperatures. *J. Phys. Chem. B* **2004**, *108*, 1529−1532.

(39) Park, J. H.; Choudhury, P.; Kummel, A. C. NO Adsorption on Copper Phthalocyanine Functionalized Graphite. *J. Phys. Chem. C* **2014**, *118*, 10076−10082.

(40) Xie, W. G.; Xu, J. B.; An, J.; Xue, K. Correlation between Molecular Packing and Surface Potential at Vanadyl Phthalocyanine/HOPG Interface. *J. Phys. Chem. C* **2010**, *114*, 19044−19047.

(41) Guillaud, G.; Simon, J.; Germain, J. P. Metallophthalocyanines - Gas Sensors, Resistors and Field Effect Transistors. *Coord. Chem. Rev.* **1998**, *178*, 1433−1484.

(42) Kong, X.-H.; Yang, Y.-L.; Lei, S.-B.; Wang, C. On the Topography Multiplicity of Non-Planar Titanyl (IV) Phthalocyanine Molecules and the STM Imaging Mechanism. *Surf. Sci.* **2008**, *602*, 684−692.

(43) Feenstra, R. M. Scanning Tunneling Spectroscopy. *Surf. Sci.* **1994**, *299−300*, 965−979.

(44) Smith, G. D.; Bedrov, D.; Borodin, O. Molecular Dynamics Simulation Study of Hydrogen Bonding in Aqueous Poly(Ethylene Oxide) Solutions. *Phys. Rev. Lett.* **2000**, *85*, 5583−5586.

(45) Passard, M.; Pauly, A.; Blanc, J.-P.; Dogo, S.; Germain, J. P.; Maleysson, C. Doping Mechanisms of Phthalocyanines by Oxidizing Gases: Application to Gas Sensors. *Thin Solid Films* **1994**, *237*, 272−276.

(46) Fukagawa, H.; Yamane, H.; Kera, S.; Okudaira, K. K.; Ueno, N. Experimental Estimation of the Electric Dipole Moment and Polarizability of Titanyl Phthalocyanine Using Ultraviolet Photoelectron Spectroscopy. *Phys. Rev. B: Condens. Matter Mater. Phys.* **2006**, *73*, 73.

(47) Schwieger, T.; Peisert, H.; Golden, M. S.; Knupfer, M.; Fink, J. Electronic Structure of the Organic Semiconductor Copper Phthalocyanine and K-CuPc Studied Using Photoemission Spectroscopy. *Phys. Rev. B: Condens. Matter Mater. Phys.* **2002**, *66*, 155207.

(48) Hill, I. G.; Kahn, A.; Soos, Z. G.; Pascal, R. A., Jr. Charge-Separation Energy in Films of π-Conjugated Organic Molecules. *Chem. Phys. Lett.* **2000**, *327*, 181−188.